

Efficient calculation of local dose distribution for response modelling in proton and ion beams

Greilich, S.^{a,*}, Hahn, U.^b, Kiderlen, M.^b, Andersen, C.E.^c, Bassler, N.^d

^a*Department of Medical Physics in Radiation Oncology, German Cancer Research
Center (DKFZ), Im Neuenheimer Feld 280, D-69120 Heidelberg, Germany*

^b*Department of Mathematical Sciences, Aarhus University, Ny Munkegade, bygning
1530, DK-8000 Aarhus C, Denmark*

^c*Center for Nuclear Technologies, Technical University of Denmark, Risø Campus, P.O.
49, DK-4000 Roskilde, Denmark*

^d*Department of Experimental Clinical Oncology, Aarhus University Hospital,
Nørrebrogade 44, DK-8000 Aarhus C, Denmark*

Abstract

We present an algorithm for fast and accurate computation of the local dose distribution in MeV beams of protons, carbon ions or other heavy-charged particles. It uses compound Poisson-process modelling of track interaction and successive convolutions for fast computation. It can handle mixed particle fields over a wide range of fluences. Since the local dose distribution is the essential part of several approaches to model detector efficiency or cellular response it has potential use in ion-beam dosimetry and radiotherapy.

Keywords: response modelling, numerical modeling, track structure theory

PACS: 78.90.+t, 87.53.-j

1. Introduction

Amorphous track models (ATMs) disregard the stochastic energy deposition pattern by secondary electrons around the track of densely ionizing, heavy charged particles (i.e. protons or ions, HCPs). Rather, they consider

*Corresponding author, Tel: +49-(0)6221-42-2632, Fax: +49-(0)6221-42-2665
Email address: s.greilich@dkfz.de (Greilich, S.)

19 an dose average as a two-dimensional, radially symmetric function of perpen-
 20 dicular distance r from the trajectory, referred to as radial dose distribution
 21 $d(r)$ (Fig. 1).

22 In contrast, sparsely ionizing radiation such as photons deposits energy by
 23 secondary electrons as well, yet ionization events are supposed to be homoge-
 24 neously distributed across the irradiated media. The 'local effect' assumption
 25 in ATMs assumes that on small scales ($\ll \mu\text{m}$) the energy deposition from
 26 HCPs cannot be distinguished from a photon field.

27 The response to irradiation with HCPs of type T and energy E can there-
 28 fore be predicted from the homogenous bulk photon dose response $S_X(D)$ of
 29 the system and the spatial deposition of local dose $d(x, y)$ as calculated from
 30 the fluences $\Phi(E, T)$ of the particle field. Despite many simplifications, ATMs
 31 are reasonably successful in predicting the response for a variety of physical
 32 detectors and biological systems [1, 2, 3, 4]. In a former study [5], we em-
 33 ployed ATMs for our all-optical dose verification system using fiber-coupled
 34 $\text{Al}_2\text{O}_3:\text{C}$ as prerequisite for use in particle beams [6, 7].

35 In [7] we used a simple generic grid summation (GSM) based on a Monte-
 36 Carlo technique. There, particles are sampled according to their relative
 37 fluence and local doses $d(x, y)$ — and therefore local response $s(x, y) =$
 38 $S_X(d(x, y))$ — are computed on a Cartesian grid ('checkerboard') by attribut-
 39 ing the corresponding $d_{E,T}(r)$ to the sampled particle (Fig. 2). The detector
 40 is thought to be homogenous, perpendicular to the beam in (x, y) , and of
 41 negligible thickness Δz . The relative efficiency η can then be estimated by
 42 averaging the local response s over all grid elements:

$$\eta(\phi(E, T)) = \frac{S_{HCP}}{S_X(D)} = \frac{\langle s \rangle}{S_X(\langle d \rangle)} \quad (1)$$

43 Although conceptually straightforward, GSM can be very time-consuming,
 44 esp. in the case of higher fluences and particle energies (e.g. $E_{\text{proton}} > 20$
 45 MeV) with many contributions to a single voxel. Furthermore, the procedure
 46 has to be repeated many times in order to converge — or a large detector
 47 grid has to be simulated.

48 **2. Computation of the local dose distribution using compound** 49 **Poisson processes**

50 To overcome the limitations of GSM calculating the local dose distribution
 51 as a spatial deposition pattern $d(x, y)$, we consider a representative point P
 52 (Fig. 2). The cumulative distribution function $F(d)$ of local dose d in P de-
 53 pends on the macroscopic fluence ϕ (and dose D , resp.) and the microscopic
 54 pattern around a track as expressed by $d(r)$. Then, one can state:

- 55 • r_{max} is the maximum secondary electron range in the field, so P is only
 56 influenced by tracks within a circle C of radius r_{max} around P (Fig. 2).
- 57 • All tracks in C are contributing to d and their number n is Poisson
 58 distributed with mean $\mu = \phi \cdot \pi r_{max}^2$.
- 59 • Let F_n be the cumulative distribution function of the local dose in the
 60 case of exactly n tracks. For a single track traversing C , we readily
 61 have the cumulative single impact distribution

$$F_1(d) = 1 - \frac{R(d)^2}{r_{max}^2}, \quad (2)$$

62 with $R(d) = D^{-1}(r)$ (Fig. 1).

- 63 • In the case of n tracks in C , d is the sum of n independent and identi-
 64 cally distributed single track doses, so F_n can be expressed as the n -fold
 65 convolution of F_1 :

$$F_n = \underbrace{F_1 * \dots * F_1}_{n \text{ times}} \quad (3)$$

- 66 • As n is Poisson distributed, F is the distribution function of a com-
 67 pound Poisson process:

$$F(d) = e^{-\mu} \sum_{i=1}^{\infty} \frac{\mu^i}{i!} F_i(d) \quad (4)$$

- 68 • The derivative $f(d)$ of $F(d)$ can then be eventually used to compute
 69 the macroscopic HCP response as the expected local response $\langle s \rangle$:

$$\langle s \rangle = \int_0^{\max(d)} S_X(d) f(d) dd, \quad (5)$$

70 and used in Eq. (1) to get the η . A similar procedure for $\langle d \rangle$ provides
 71 a quality check as it has to meet D .

72 This description enables F to be determined from the explicitly given distri-
 73 bution function F_1 in the case of monoenergetic particle fields. It can easily
 74 be extended to mixed particle fields by using the adjusted F_1 from Eq.(6) in
 75 Eq.(3) with $p_{E,T}$ being the relative fluence and $R_{E,T}$ the inverse radial dose
 76 distribution for the composing particles

$$F_1(d) = 1 - \sum_{E,T} p_{E,T} \cdot \frac{R_{E,T}(d)^2}{\hat{r}_{max}^2}, \quad (6)$$

77 where $\hat{r}_{max} = \max(r_{max}(E, T))$.

78 It should be stressed that the presented approach is in no way limited to
 79 handle extended targets despite the point nature of P as the averaging across

80 the target is already contained in $D(r)$ (for the difference between point and
 81 extended target distributions, see [1, 6]). While the computation of detec-
 82 tor response from the local dose distribution $F(d)$ is trivial, the numerical
 83 calculation of $F(d)$ itself can, however, be cumbersome.

84 3. Accelerated computation using successive convolution

85 An approximation method for the rapid computation of compound Pois-
 86 son processes was introduced by Kellerer [8]. It makes use of the fact that
 87 the distribution $f(d; \mu)$ can be obtained by a convolution operation:

$$f(d; \mu) = \int_0^d f(d-t; \mu/2) \cdot f(t; \mu/2) dt \quad (7)$$

88 One can chose a $\mu_{start} \ll 1$ with $\mu = 2^m \cdot \mu_{start}$ so that multiple events
 89 can be neglected and therefore $f(d; \mu_{start})$ consists, in good approximation,
 90 of two components only, namely the probability of no track in C ($d = 0$)

$$e^{-\mu_{start}} \approx (1 - \mu_{start}) = \hat{f}_0 \quad (8)$$

91 and of the density related to a single track

$$\hat{f}_1 \approx \mu_{start} \cdot f_1(d). \quad (9)$$

92 Performing m successive convolutions on these two components, i.e. replacing

$$\hat{f}_0 \text{ by } \hat{f}_0^2 \quad (10)$$

93 and

$$\hat{f}_1 \text{ by } 2 \cdot \hat{f}_0 \cdot \hat{f}_1 + \hat{f}_1 * \hat{f}_1 \quad (11)$$

94 will eventually yield $f(d)$.

95 4. Results and conclusion

96 Fig. 3 shows that the new algorithm delivers $f(d)$ — as the essential part
97 of modelling detector efficiency and cellular response in HCP beams — in
98 very good agreement with GSM but significantly faster. In addition, it covers
99 a much wider range of local dose and can handle high energy (i.e. very wide)
100 tracks like the 30 MeV component in the mixed field that clearly overstrains
101 the capabilities of GSM. The novel algorithm presented thus allows a much
102 larger parameter space in ATM modelling. Using it, spatial binning becomes
103 obsolete. In addition, even complex particle fields can easily be treated as
104 they mainly affect the computation of F_1 , the number of convolutions. We
105 believe that the algorithm can contribute to the applicability of ATMs and
106 the improvement of accuracy in their predictions for HCP dosimetry and
107 radiotherapy. It has been implemented as part of the open-source project
108 libamtrack (<http://libamtrack.dkfz.org>).

109 Acknowledgments

110 The authors gratefully acknowledge the support by CIRRO (The Lund-
111 beck Foundation Center for Interventional Research in Radiation Oncology)
112 and The Danish Council for Strategic Research. NB acknowledges sup-
113 port from the Danish Cancer Society and the German Research Foundation
114 (DFG).

115 **References**

116 **References**

- 117 [1] R. Katz, S. C. Sharma, and M. Homayoonfar. The structure of particle
118 tracks. In F. H. Attix, editor, *Topics in Radiation Dosimetry*, chapter 6,
119 pages 317–383. Academic Press, New York, 1972.
- 120 [2] M.P.R. Waligórski and R. Katz. Supralinearity of peak 5 and peak 6 in
121 TLD-700. *NIM*, 172:463–470, 1980.
- 122 [3] O. B. Geiß, M. Krämer, and G. Kraft. Efficiency of thermoluminescence
123 detectors to heavy charged particles. *NIM B*, 142:592–598, 1998.
- 124 [4] N. Bassler, J.W. Hansen, H. Palmans, M.H. Holzscheiter, S. Kovacevic,
125 and the AD-4/ACE Collaboration. The antiproton depthdose curve mea-
126 sured with alanine detectors. *NIM B*, 266:929–936, 2008.
- 127 [5] C.E. Andersen, S.K. Nielsen, S. Greilich, J. Helt-Hansen, J.C. Linde-
128 gaard, and K. Tanderup. Characterization of a fiber-coupled $\text{Al}_2\text{O}_3\text{:C}$
129 luminescence dosimetry system for online in vivo dose verification during
130 ^{192}Ir brachytherapy. *Med. Phys.*, 36:708–718, 2009.
- 131 [6] J. Edmund, C. Andersen, and S. Greilich. A track structure model of
132 optically stimulated luminescence from $\text{Al}_2\text{O}_3\text{:C}$ irradiated with 10-60
133 MeV protons. *NIM B*, 21:261–275, 2007.
- 134 [7] S. Greilich, J.M. Edmund, M. Jain, and C.E. Andersen. A coupled RL
135 and transport model for mixed-field proton irradiation of $\text{Al}_2\text{O}_3\text{:C}$. *Rad.*
136 *Meas.*, 43:10491053, 2008.

137 [8] A.M. Kellerer. Fundamentals of microdosimetry. In K.R. Kase, B.E.
138 Bjärngard, and F.H. Attix, editors, *The Dosimetry of Ionizing Radiation*,
139 chapter 2. Academic Press, London, 1985.

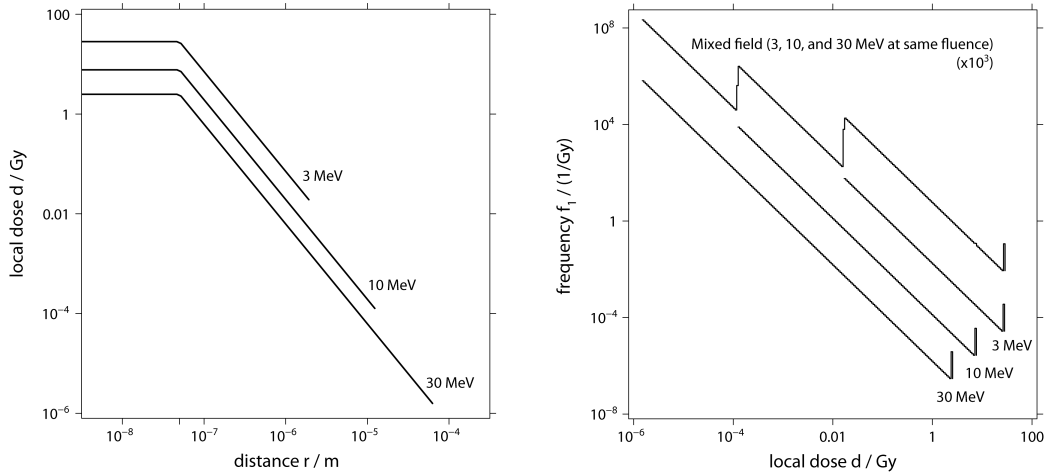


Figure 1: Left: Radial dose distributions $d(r)$ in water for three proton energies. Considerable differences exist between parameterizations from different authors. For simplicity, we use the one by Scholz as in [6]. Right: Single impact distributions $f_1(d)$ for the same particles plus a mixed field case (for visibility scaled by 10^3) with logarithmic binning (10 bins per factor of 10). Although relatively unlikely, high local doses in the core region can contribute significantly to the total dose (tens of percent) and must not be neglected.

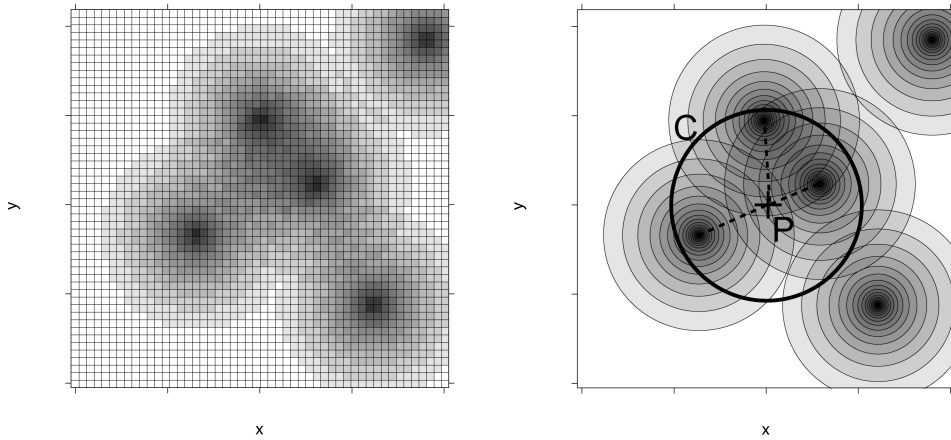


Figure 2: Illustration of the GSM (left) and the compound Poisson modelling.

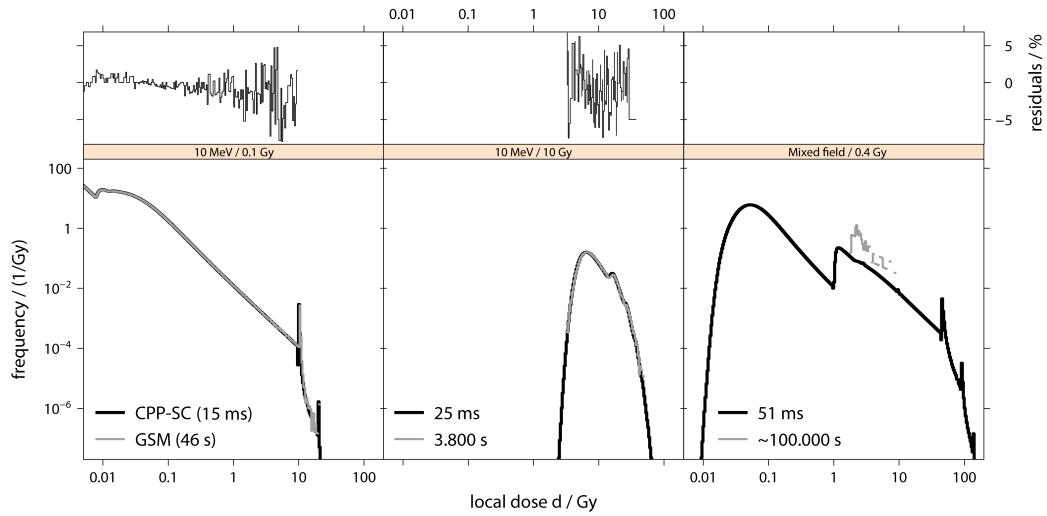


Figure 3: Comparison of the resulting local dose distribution $f(d)$ from GSM and the algorithm based on compound Poisson processes using successive convolutions (CPP-SC). Left: At low fluence the structure of $f_1(d)$ still visible, but a low dose dip and multiple core events occur due to track overlap. Middle: High fluence case. With many contribution tracks, $f(d)$ approaches a narrow Gaussian profile corresponding to a homogenous dose over the detector ('sea of electrons'). Right: Mixed field case (as in Fig. 1). For GSM, normalization fails due to edge effects.